

## Silver-catalyzed bioleaching of enargite concentrate using moderately thermophilic microorganisms

Oyama, Keishi

Department of Earth Resource Engineering, Faculty of Engineering, Kyushu University

Shimada, Kazuhiko

Department of Earth and Planetary Sciences, Faculty of Science, Kyushu University

Ishibashi, Jun-ichiro

Department of Earth and Planetary Sciences, Faculty of Science, Kyushu University

Miki, Hajime

Department of Earth Resource Engineering, Faculty of Engineering, Kyushu University

他

<https://hdl.handle.net/2324/4737398>

---

出版情報 : Hydrometallurgy. 177, pp.197-204, 2018-05. Elsevier

バージョン :

権利関係 :



*Hydrometallurgy (IBS Special Issue)*

Title:

Silver-catalyzed bioleaching of enargite concentrate using moderately thermophilic microorganisms

Keishi OYAMA<sup>a</sup>, Kazuhiko SHIMADA<sup>b</sup>, Jun-ichiro ISHIBASHI<sup>b</sup>, Hajime MIKI<sup>a</sup>,  
Naoko OKIBE<sup>a\*</sup>

<sup>a</sup> Department of Earth Resource Engineering, Faculty of Engineering, Kyushu University, 744 Motoooka, Nishi-ku, Fukuoka 819-0395, Japan

<sup>b</sup> Department of Earth and Planetary Sciences, Faculty of Science, Kyushu University, 744 Motoooka, Nishi-ku, Fukuoka 819-0395, Japan

\*Corresponding author

Tel. and Fax: +81 92 802 3312

E-mail address: okibe@mine.kyushu-u.ac.jp (Naoko OKIBE)

**Keywords:** enargite, bioleaching, silver catalyst, solution redox potential, kinetics, moderately thermophilic microorganisms

## Abstract

Effect of silver (Ag) catalyst in bioleaching of enargite ( $\text{Cu}_3\text{AsS}_4$ ) concentrate was studied using mixed cultures of moderately thermophilic acidophilic microorganisms at  $45^\circ\text{C}$ . Addition of  $\text{Ag}_2\text{S}$  enabled selective Cu dissolution from enargite while suppressing pyrite oxidation: At the highest  $\text{Ag}_2\text{S}$  concentration of 0.04%, Cu recovery reached 96% while Fe dissolution was suppressed to reach only 29% by day 72. Overall results from thermodynamic calculation, liquid/solid analyses and kinetic study suggested that Ag-catalyzed bioleaching of enargite concentrate proceeds via formation of at least two types of secondary products (chalcocite,  $\text{Cu}_2\text{S}$ ; trisilver arsenic sulfide,  $\text{Ag}_3\text{AsS}_4$ ): Addition of  $\text{Ag}_2\text{S}$  as Ag catalyst thermodynamically and microbiologically contributed to lowering solution redox potentials during bioleaching, consequently satisfying  $E_{\text{ox}}(\text{Cu}_2\text{S}) < E_h < E_c(\text{Ag}^+)$  to enhance enargite dissolution via formation of chalcocite intermediate. Formation of trisilver arsenic sulfide and its intermediate layer  $(\text{Cu,Ag})_3\text{AsS}_4$  indicated that Cu ion in the enargite lattice is gradually substituted with Ag. Such secondary products did not impose a rate-limiting step, since the Ag-catalyzed bioleaching was shown to be controlled by a chemical surface reaction, rather than diffusion through product film which was the case in the absence of  $\text{Ag}_2\text{S}$ .

## 1. Introduction

Recent depletion of high-grade copper ores has been directing researchers' attention towards utilization of low-grade and refractory copper sulfides such as chalcopyrite ( $\text{CuFeS}_2$ ) and enargite ( $\text{Cu}_3\text{AsS}_4$ ). In order to improve dissolution efficiency of such minerals, different approaches have been investigated including pressure leaching (Ruiz et al., 2011; Padilla et al., 2015), chemical acid leaching (Safarzadeh and Miller, 2014) and biological leaching (Acevedo et al., 1998; Sasaki et al., 2009). Bioleaching is expected to be one of the most promising approaches in targeting such refractory ores/concentrates, and in fact, high-temperature bioleaching ( $60\text{-}70^\circ\text{C}$ ) generally resulted in high copper recoveries (52-91%; Escobar et al., 2000; Muñoz et al., 2006; Lee et al., 2011; Takatsugi et al., 2011; Sasaki et al., 2011). Whilst at low-temperatures ( $25\text{-}30^\circ\text{C}$ ), bioleaching still remains to be improved ( $< 15\%$ ; Escobar et al., 1997; Sasaki et al., 2010). These results suggest that addition of reaction catalyst would be useful in low-temperature bioleaching to realize better copper recovery.

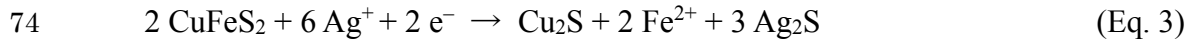
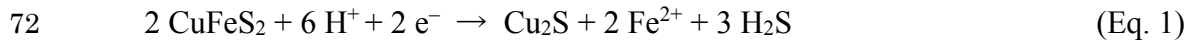
In the case of chalcopyrite bioleaching, the catalytic effect of different metal ions has been studied so far. Among those metals tested, Ag ion was found to be effective in catalyzing chalcopyrite dissolution, whereas Co, Mn, Sb, Bi, Ni and Sn ions

showed weak or no catalytic abilities (Ballester et al., 1990; Muñoz et al., 2007).

The mechanism of Ag-catalyzed chalcopyrite leaching has been explained by different research groups based on abiotic leaching studies, such as via (i) improvement of electrical conductivity by formation of Ag<sub>2</sub>S inside S<sup>0</sup> layer on the chalcopyrite surface (Nazari et al., 2012), (ii) Ag atom diffusion into the metal-deficient sulfur-rich passive layer formed on the chalcopyrite surface (Ghahremaninezhad et al., 2015) and (iii) Ag<sub>2</sub>S formation which rapidly consumes H<sub>2</sub>S produced via intermediate chalcocite (Cu<sub>2</sub>S) formation from chalcopyrite, indirectly accelerating chalcopyrite dissolution (Hiroyoshi et al., 2002). The third theory was proposed by detailed electrochemical/chemical studies and thermodynamic calculations, revealing the correlation between the Ag-catalyzed chalcopyrite dissolution behavior and solution redox potential (Eh). Formation of intermediate Cu<sub>2</sub>S (Eq. 3; sum of Eq. 1 and 2) and its oxidation to yield Cu<sup>2+</sup> (Eq. 4) proceed simultaneously, when Eh satisfies the optimal range of  $E_{ox} < Eh < E_c$ .

$E_c$  (“critical potential”): the equilibrium redox potential for the intermediate chalcocite formation from chalcopyrite

$E_{ox}$  (“oxidation potential”): the equilibrium redox potential for the subsequent oxidation of chalcocite to Cu<sup>2+</sup>



76 As for enargite leaching, studies on the mechanism of Ag catalyst are still  
77 highly limited. An electrochemical study by Miki et al. (2016) suggested that addition of  
78 Ag expands the optimal Eh range, which allows enhanced enargite dissolution. However,  
79 the detailed mechanism is yet unclear and its effect in bioleaching is largely unknown.  
80 Although the use of Ag catalyst is considered unpractical for copper extraction,  
81 clarifying its catalytic mechanism would be beneficial in understanding how enargite  
82 leaching can be facilitated.

83 The objectives of this study were therefore set to evaluate the catalytic effect of  
84 Ag on bioleaching of enargite concentrate and to elucidate its mechanism.

85

## 2. Materials and Methods

### 2.1. Microorganisms

Three bacterial strains (*Acidimicrobium ferrooxidans* ICP (DSM 10331); *Sulfobacillus sibiricus* N1 (DSM 17363); *Acidithiobacillus caldus* KU (DSM 8584)) and an archaeal strain (*Ferroplasma acidiphilum* Y (DSM 12658)) were employed in this study based on their synergistic effect found in arsenic-bearing solutions during arsenopyrite biooxidation (Tanaka et al., 2015). They were routinely cultivated under aerobic condition in 500 mL Erlenmeyer flasks containing 200 mL of heterotrophic basal salts (HBS) medium (0.5 g/L  $\text{MgSO}_4 \cdot 7\text{H}_2\text{O}$ , 0.45 g/L  $(\text{NH}_4)\text{SO}_4$ , 0.05 g/L KCl, 0.05 g/L  $\text{KH}_2\text{PO}_4$ , 0.014 g/L  $\text{Ca}(\text{NO}_3)_2 \cdot 4\text{H}_2\text{O}$ , 0.142 g/L  $\text{Na}_2\text{SO}_4$ ; pH 1.5 with  $\text{H}_2\text{SO}_4$ ). For *Am. ferrooxidans* ICP and *Sb. sibiricus* N1, 0.02% (w/v) yeast extract plus 10 mM  $\text{Fe}^{2+}$  (added as  $\text{FeSO}_4 \cdot 7\text{H}_2\text{O}$ ) were added. For *Fp. acidiphilum* Y, 0.02% yeast extract plus 20 mM  $\text{Fe}^{2+}$  were added. For *At. caldus* KU, 0.5 g  $\text{S}^0$  plus 200  $\mu\text{L}$  of trace elements stock solution (10 mg/L  $\text{ZnSO}_4 \cdot 7\text{H}_2\text{O}$ , 1 mg/L  $\text{CuSO}_4 \cdot 5\text{H}_2\text{O}$ , 1.09 mg/L  $\text{MnSO}_4 \cdot 5\text{H}_2\text{O}$ , 1 mg/L  $\text{CoSO}_4 \cdot 7\text{H}_2\text{O}$ , 0.39 mg/L  $\text{Cr}_2(\text{SO}_4)_3 \cdot 7\text{H}_2\text{O}$ , 0.6 mg/L  $\text{H}_2\text{BO}_3$ , 0.5 mg/L  $\text{Na}_2\text{MoO}_4 \cdot 2\text{H}_2\text{O}$ , 0.1 mg/L  $\text{NaVO}_3$ , 1 mg/L  $\text{NiSO}_4 \cdot 6\text{H}_2\text{O}$ , 0.51 mg/L  $\text{Na}_2\text{SeO}_4$ , 0.1 mg/L  $\text{Na}_2\text{WO}_4 \cdot 2\text{H}_2\text{O}$ ) were added. Flasks were incubated at 45°C, shaken at 150 rpm.

## 2.2. Minerals

The enargite concentrate ( $P_{80} = 90 \mu\text{m}$ ) used in this study was from Peru, consisting of enargite ( $\text{Cu}_3\text{AsS}_4$ ) 37.4%, pyrite ( $\text{FeS}_2$ ) 47.3%, tennantite ( $(\text{Cu,Fe})_{12}\text{As}_4\text{S}_{13}$ ), chalcopyrite ( $\text{CuFeS}_2$ ), sphalerite ( $\text{ZnS}$ ), stibnite ( $\text{Sb}_2\text{S}_3$ ) and quartz ( $\text{SiO}_2$ ). The elemental composition of enargite concentrate was as follows; S 39%, Fe 22%, Cu 20%, As 7.1%, Zn 0.39%, Sb 0.32%, Al 0.22%. Prior to bioleaching experiments, the enargite concentrate was washed sequentially with 1 M  $\text{HNO}_3$ , deionized water and ethanol.

## 2.3. Bioleaching experiments

Pre-grown cells of each of four strains were collected by centrifugation (9000 rpm, 10 min at  $4^\circ\text{C}$ ) and washed twice with acidified water (pH 1.7 with  $\text{H}_2\text{SO}_4$ ), prior to inoculation into 200 mL HBS medium (pH 2.0 with  $\text{H}_2\text{SO}_4$ ; in 500 mL Erlenmeyer flasks) containing 2% (w/v) enargite concentrate and 5 mM  $\text{Fe}^{2+}$ , so as to set the initial cell density of each strain at  $1.0 \times 10^7$  cells/mL (i.e.  $4.0 \times 10^7$  cells/mL in total). Silver sulfide ( $\text{Ag}_2\text{S}$ ), instead of soluble silver salts, was added as Ag catalyst into the medium at different concentrations, 0, 0.005, 0.01, 0.02, 0.03 and 0.04% (w/v), owing to the low solubility of  $\text{Ag}^+$  ions (Goates et al., 1951; Hseu and Rechnitz, 1968; Supplemental Fig. 1) which transform immediately to  $\text{Ag}_2\text{S}$  in leaching solutions (Miki et al., 2016). Flasks were incubated shaken at  $45^\circ\text{C}$  and 150 rpm for 72 days. Samples were regularly withdrawn to monitor pH, Eh, cell density and concentrations of  $\text{Fe}^{2+}$ , total Fe, As and



Cu.

#### 2.4. Analytical methods

Liquid samples were filtered (0.20  $\mu\text{m}$ ) to measure concentrations of total Cu, Fe and As by inductively coupled plasma optical emission spectrometry (ICP-OES; PerkinElmer Optima 8300DV), and  $\text{Fe}^{2+}$  by the *o*-phenanthroline method. Leaching residues were collected after bioleaching and freeze-dried overnight for X-ray diffraction (XRD; Rigaku Ultima IV;  $\text{CuK}\alpha$  40 mA, 40 kV) analysis. For quantitative elemental composition analysis by electron probe micro analyzer (EPMA; JOEL JXA-8530F; 6 nA, 20 kV), the leaching residues were embedded into resin and polished. Incident electron beam was focused to 1  $\mu\text{m}$  in diameter and counting time was set to 20 sec for each element. The acquired results were collected by ZAF method (Boekestein et al., 1983).

#### 2.5. Real-time PCR

In order to investigate the microbial population structure in bioleaching cultures, real-time PCR (Bio-Rad MiniOpticon) was conducted according to the methods described by Tanaka et al. (2015) with some modifications as follows: The purified genomic DNA from each strain was used as the template to PCR-amplify the

16S rRNA gene fragment (~1473 bp) using the universal primer set (27f and 1492r for bacteria or Arch 21f and 1492r for archaea: Table 1). The resultant PCR products derived from each strain were purified (NIPPON GENE ISOSPIN PCR Product), quantified, and finally diluted to give a final concentration of  $1.0 \times 10^3$  to  $1.0 \times 10^9$  copies/ $\mu$ L, to be used as template DNA for real-time PCR. Once linearity in the standard curve was obtained within the range from  $1.0 \times 10^3$  to  $1.0 \times 10^9$  copies/ $\mu$ L for all species, synthetic DNA mixtures (composed of template DNA from each one of the four species at  $1.0 \times 10^3$  to  $1.0 \times 10^9$  copies/ $\mu$ L) were tested against each one of the four species-specific primer sets (Table 1) to ensure the accuracy in order to display the results as percentages in whole number. Genomic DNA extracted from the actual bioleaching mixed cultures were tested against the corresponding species-specific primer sets.

### 3. Results and Discussion

#### 3.1. Dissolution behavior of Cu, Fe and As during bioleaching with and without Ag<sub>2</sub>S

In the absence of Ag<sub>2</sub>S, Cu recovery was 43% on day 72 (Fig. 1a), while Fe started to dissolve mainly from pyrite on day 10 to a rapid completion (100%) by day 40 (Fig. 1c), accompanied by a stably high Eh at around 770 mV (Fig. 1e). This high redox condition supported pyrite dissolution whereas enargite oxidation was hindered due to the formation of passivation layer such as jarosite (Muñoz et al., 2006; Takatsugi et al., 2011). Increasing addition of Ag<sub>2</sub>S (0.005-0.04%) led to consecutively greater Cu recoveries (Fig. 1a) and lower Fe dissolutions (Fig. 1c), with Fe<sup>2+</sup> oxidation seemingly being increasingly delayed (Fig. 1d) and thus Eh values being increasingly suppressed (Fig. 1e). The results thus indicate that Ag<sub>2</sub>S addition improves Cu recovery by enabling selective Cu dissolution from enargite concentrate. Selective suppression of pyrite dissolution has been also reported in Ag-catalyzed chalcopyrite bioleaching studies (Ahonen and Tuovinen, 1990; Ballester et al., 1990). As for cell growth, active cell growth was seen despite of the presence of antibacterial effect of Ag<sup>+</sup> (Marambio-Jones and Hoek, 2010). Rather, addition of Ag<sub>2</sub>S was found effective in maintaining high cell densities which otherwise decreased towards the end of stationary phase (Fig. 1f). At the highest Ag<sub>2</sub>S concentration of 0.04%, Cu recovery reached 96% (Fig. 1a) while Fe

dissolution was suppressed to reach only 29% by day 72 (Fig. 1c). Under this condition, 56% of dissolved As was calculated to be re-immobilized during bioleaching by day 72, compared with 36% As re-immobilization observed in the absence of Ag<sub>2</sub>S (Fig. 1b) (calculated based on the theoretical amount of As solubilized from enargite at the ratio of Cu:As = 3:1).

XRD analysis of the original enargite concentrate (Fig. 2a) and bioleached residues (Fig. 2b-g) indeed showed the trend that enargite peaks selectively and progressively diminished, while leaving pyrite peaks increasingly unchanged at higher Ag<sub>2</sub>S concentrations. Jarosite (KFe<sub>3</sub>(SO<sub>4</sub>)<sub>2</sub>(OH)<sub>6</sub>) peaks were found after bioleaching only in the absence of Ag<sub>2</sub>S (Fig. 2b), where pyrite was selectively and completely dissolved by day 40 (Fig. 1c). During bioleaching, fine red precipitates floating on the bioleaching liquors became increasingly visible at higher Ag<sub>2</sub>S concentrations. Although no XRD peaks attributing As secondary minerals were detected when bulk bioleached residue samples were analyzed (Fig. 2), selective recovery of the red precipitates enabled their identification by XRD as trisilver arsenic sulfide (Ag<sub>3</sub>AsS<sub>4</sub>) (Fig. 3).

### 3.2. Suppression of pyrite dissolution by Ag<sub>2</sub>S

The effect of Ag<sub>2</sub>S in selective suppression of pyrite dissolution can be attributed to the following reasons; (i) the change in microbial population structure due to inhibitory effect of Cu<sup>2+</sup> and/or antibacterial Ag<sup>+</sup> ions, causing the low solution redox condition, (ii) the difference in rest potentials of co-existing minerals (enargite, pyrite and Ag<sub>2</sub>S) displaying different subjectivity to oxidation.

As for (i), the real-time PCR analysis found that Fe-oxidizing *Am. ferrooxidans* ICP was the dominant species in the absence of Ag<sub>2</sub>S (97-75% on day 15-30; Fig. 4). However, addition of 0.04% Ag<sub>2</sub>S decreased its abundance to 57-31% whereas S-oxidizing *At. caldus* KU became the dominant species by increasing its ratio from 1-5% (0% Ag<sub>2</sub>S) to 42-53% (0.04% Ag<sub>2</sub>S) (on day 15-30; Fig. 4). The lower tolerance of *Am. ferrooxidans* ICP (9 mM) than *At. caldus* KU (24 mM) to Cu<sup>2+</sup> (Watkin et al., 2009) may be responsible for this observation, as Cu dissolution advanced steadily to reach 19-37 mM on day 15-30 when 0.04% Ag<sub>2</sub>S was added (in contrast to 13-18 mM at 0% Ag<sub>2</sub>S; Fig. 1a). The abundance of *Sb. sibiricus* N1 became noticeable at the later stage of bioleaching both at 0% and 0.04% Ag<sub>2</sub>S (Fig. 4), probably resulting from its extremely high tolerance to Cu<sup>2+</sup> (299 mM) and As(V) (100 mM) (Watling et al., 2008). The population of *Fp. acidiphilum* Y did not emerge throughout the experiment in both cases, probably due to its sensitivity to the temperature condition used here (Golyshina

et al., 2000). There may also have been an antibacterial effect of  $\text{Ag}^+$  to the microbes used, but their individual sensitivity to  $\text{Ag}^+$  is unclear.

This difference in microbial population structure resulted in deterioration of microbial  $\text{Fe}^{2+}$  oxidation in the presence of  $\text{Ag}_2\text{S}$ , which may have partly caused the apparent delay of pyrite oxidation (Fig. 1c) and the suppression of Eh values (Fig. 1e).

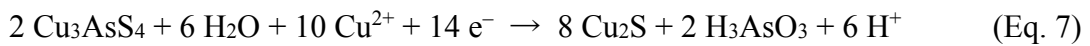
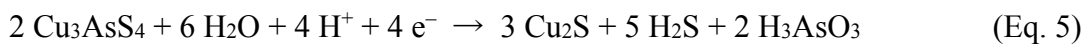
As for (ii), rest potentials of the minerals were reported to be as follows: 164 mV vs. SCE (408 mV vs. SHE) for enargite, 398 mV vs. SCE (642 mV vs. SHE) for pyrite (Rivera-Vasquez and Dixon, 2015) and 280 mV (vs. SHE) for  $\text{Ag}_2\text{S}$  (Majima, 1969). Therefore, consumption of the oxidant,  $\text{Fe}^{3+}$ , may have been more readily directed towards oxidation of  $\text{Ag}_2\text{S}$  to release  $\text{Ag}^+$  ions, rather than to oxidation of pyrite. Due to the low solubility product of  $\text{Ag}_2\text{S}$  (Goates et al., 1951; Hseu and Rechnitz, 1968), solubilized  $\text{Ag}^+$  ions would have been immediately transformed back to  $\text{Ag}_2\text{S}$ , which is then re-oxidized by  $\text{Fe}^{3+}$ . This continuous  $\text{Ag}_2\text{S}$ -oxidation coupled with  $\text{Fe}^{3+}$ -reduction may have caused the apparent lag-time of  $\text{Fe}^{2+}$  oxidation (Fig. 1d) and the suppression of Eh values (Fig. 1e).

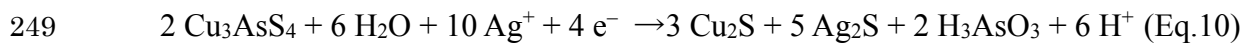
Since pyrite bioleaching favors high redox potential conditions, the above effects would likely have contributed to suppression of pyrite bioleaching.

### 3.3. Promotion of enargite dissolution by Ag<sub>2</sub>S

The theory of Ag-catalyzed chalcopyrite leaching (Hiroyoshi et al., 2002) was applied to that of Ag-catalyzed electrochemical enargite leaching by Miki et al. (2016), suggesting the existence of the optimal Eh range for enhanced enargite dissolution as follows:

In the absence of Ag, when Eh is within the optimal range, enargite dissolution proceeds via formation of intermediate Cu<sub>2</sub>S (Eq. 5) and H<sub>2</sub>S generated by Eq. 5 is consumed by Cu<sup>2+</sup> to form Cu<sub>2</sub>S (Eq. 6). The overall reaction of Eq. 5 and 6 can be summarized as Eq. 7 and the resultant Cu<sub>2</sub>S is amenable to oxidation to produce Cu<sup>2+</sup> (Eq. 8). However, this optimal range is narrow and exists at the relatively lower redox potential level (0.501-0.503 V; Miki et al., 2016), implying that Eq. 7 and 8 hardly occur simultaneously in general bioleaching cultures. If Ag is present, however, H<sub>2</sub>S generated by Eq. 5 is immediately removed by Ag<sup>+</sup> to form Ag<sub>2</sub>S (Eq. 9) to result in Eq. 10 (the sum of Eq. 5 and Eq. 9), leading to expansion of the optimal Eh range (0.501-1.020 in the presence of 10<sup>-5</sup> M Ag<sup>+</sup>; Miki et al., 2016).





250 The optimal Eh ranges in the absence and presence of Ag are expressed as Eq. 11 and  
251 12, respectively.

252 
$$E_{\text{ox}}(\text{Cu}_2\text{S}) < E_h < E_c(\text{Cu}^{2+}) \quad (\text{Eq. 11})$$

253 
$$E_{\text{ox}}(\text{Cu}_2\text{S}) < E_h < E_c(\text{Ag}^+) \quad (\text{Eq. 12})$$

254  $E_c(\text{Cu}^{2+})$  and  $E_c(\text{Ag}^+)$  (“critical potential”): the equilibrium redox potential for the  
255 intermediate  $\text{Cu}_2\text{S}$  formation from enargite in the absence (Eq. 7) and presence (Eq. 10)  
256 of Ag, respectively

257  $E_{\text{ox}}(\text{Cu}_2\text{S})$  (“oxidation potential”): the equilibrium redox potential for the subsequent  
258 oxidation of  $\text{Cu}_2\text{S}$  to  $\text{Cu}^{2+}$  (Eq. 8).

259 In order to estimate whether or not the above  $\text{Cu}_2\text{S}$  intermediate reaction  
260 contributed to enargite bioleaching in this study, actual measured values were evaluated  
261 if they satisfy Eq. 11 and/or 12. Actual As(III) concentrations were not measured in this  
262 study. Therefore, calculations for  $E_c(\text{Cu}^{2+})$ ,  $E_c(\text{Ag}^+)$  and  $E_{\text{ox}}(\text{Cu}_2\text{S})$  values were  
263 conducted (as described in Supplemental Table 1) based on both assumptions that (i)  
264 total As concentrations equal to As(III) concentrations (Supplemental Table 1) and (ii)



As(III) concentrations are negligible ( $10^{-5}$  M) (Supplemental Table 2), in order to ensure that the results are similar in both cases. Copper extraction rates and  $E_{\text{have}}$  values were calculated using Eq. 13 and 14, respectively, and listed in Supplemental Tables 1 and 2.

$$\text{Cu extraction rate} = \frac{X_n - X_{n-1}}{t_n - t_{n-1}} \quad (\text{Eq. 13})$$

$$E_{\text{have}} = \frac{E_{h_n} + E_{h_{n-1}}}{2} \quad (\text{Eq. 14})$$

$t_n$ : the sampling time (day)

$X_n$ : total dissolved Cu concentration on day  $t_n$  (M)

$E_{h_n}$ : Eh value on day  $t_n$  (V vs. SHE)

The calculated  $E_c(\text{Cu}^{2+})$  values in all cultures were 0.588-0.607 V and 0.607-0.633 V as shown in Supplemental Tables 1 and 2, respectively. These values were only about maximum of 0.1 V higher than the  $E_{\text{ox}}(\text{Cu}_2\text{S})$  values (0.501-0.524 V; Supplemental Tables 1 and 2). Measured  $E_{\text{have}}$  values could hardly locate within this < 0.1 V-wide optimal range, indicating that enargite dissolution was hardly contributed by the  $\text{Cu}_2\text{S}$  intermediate reaction in the absence of Ag.

In the presence of Ag, this optimal range was greatly expanded due to the higher redox potential of  $E_c(\text{Ag}^+)$ : 1.044-1.500 V and 1.120-1.590 V (Supplemental Tables 1 and 2, respectively). The correlation between  $E_{\text{have}}$  values and Cu extraction rates was plotted in Fig. 5, by employing the maximum  $E_{\text{ox}}(\text{Cu}_2\text{S})$  value of 0.524 V and

the minimum value of  $E_c(\text{Ag}^+)$  (1.044 V) as the strictest evaluation (Supplemental Tables 1 and 2). All plots were within the optimal range satisfying  $E_{\text{ox}}(\text{Cu}_2\text{S}) < E_h < E_c(\text{Ag}^+)$  (Eq. 12), with generally higher Cu extraction rates at elevated  $\text{Ag}_2\text{S}$  concentrations (Fig. 5). The results suggest that the  $\text{Cu}_2\text{S}$  intermediate reaction was involved in enargite bioleaching in the presence of  $\text{Ag}_2\text{S}$ .

#### *3.4. Copper substitution on enargite surface with silver*

Following identification of trisilver arsenic sulfide by XRD (Fig. 3), EPMA elemental mapping was performed in order to confirm formation of Ag-containing passivation layers around the enargite surface after bioleaching with 0.04%  $\text{Ag}_2\text{S}$  (Fig. 6). Emergence of bright white areas on the enargite surface indicated formation of secondary minerals consisting of heavier metals than Cu, such as Ag (Fig. 6a). The enargite grain was indeed covered with a thick but porous secondary layer (Fig. 6a; solid arrow), consisting of Ag, As and S (Fig. 6b, d, e), onto which another partial layer (Fig. 6a; broken arrow) of ferric arsenate (Fig. 6d, f) was observed.

To further analyze the formation of Ag-containing passivation layers, EPMA quantitative analysis was conducted on different locations of the particle (Fig. 7): Spot 1, the core of enargite grain (grey); Spot 4, the passivation layer around the enargite

surface (white); Spots 2 and 3, the interface between Spots 1 and 4 (light grey). Spots 1-4 shared the approximate atomic ratio of  $(\text{Cu} + \text{Ag}) : \text{As} : \text{S} = 3 : 1 : 4$ , with different Ag : Cu ratios (Table 2). An increasing dominance of Ag relative to Cu, from the core to surface of the enargite particle indicated that Cu was dissolved from enargite ( $\text{Cu}_3\text{AsS}_4$ ; Spot 1) possibly by substitution with Ag ( $(\text{Cu},\text{Ag})_3\text{AsS}_4$ ; Spots 2 and 3), eventually leaving the passivation layer of trisilver arsenic sulfide ( $\text{Cu}_3\text{AsS}_4$ ; Spot 4) (Fig. 7).

In chemical/electrochemical studies for chalcopyrite, metal-deficient sulfur-rich layers ( $\text{Cu}_{1-x}\text{Fe}_{1-y}\text{S}_2$  or  $\text{Cu}_{1-x}\text{Fe}_{1-y}\text{S}_{2-z}$ ) were reported to passivate the mineral surface (Warren et al., 1982; Hackl et al., 1995; Ghahremaninezhad et al., 2010, 2013). Ghahremaninezhad et al. (2015) explained the mechanism of Ag-catalyzed chalcopyrite dissolution by Ag diffusion into such metal-deficient sulfur-rich layers, eventually producing  $\text{Ag}_2\text{S}$  passivation. Likewise, trisilver arsenic sulfide detected in this study might have been formed via Ag ion diffusion into enargite-type metal-deficient sulfur-rich layers ( $\text{Cu}_{3-x}\text{AsS}_4$ ; Córdova et al., 1997; Fantauzzi et al., 2007, 2009).

### *3.5. Kinetic study on Ag-catalyzed bioleaching of enargite concentrate*

The shrinking core model is frequently utilized to model the mineral dissolution process. Based on this model, the dissolution reaction proceeds either via

diffusion through liquid film (Eq. 15), diffusion through product film (Eq. 16) or surface chemical reaction (Eq. 17), one of which may become the rate-limiting step under certain conditions (Wadsworth and Sohn, 1979).

$$X = k_l t \quad (\text{Eq. 15})$$

$$1 - 3(1 - X)^{2/3} + 2(1 - X) = k_d t \quad (\text{Eq. 16})$$

$$1 - (1 - X)^{1/3} = k_r t \quad (\text{Eq. 17})$$

$X$ : the fraction of dissolved Cu

$t$ : the reaction time

$k$ : the rate constant

In order to investigate which process **rate-limits** Cu dissolution during bioleaching of enargite concentrate with and without Ag<sub>2</sub>S, measured values from Fig. 1a were fitted to Eq. 16 and 17 (Fig. 8). The fluid film resistance was considered negligible relative to other effects and in fact no linear relationships between  $X$  against  $t$  were found (data not shown). The  $k$  and  $R^2$  values were calculated from the fitting results and listed in Table 3. Linear lines were drawn where  $R^2$  values of regression analyses were  $> 0.99$  (Fig. 8).

In the absence of Ag<sub>2</sub>S, rapid Fe dissolution (Fig. 1c) caused precipitation of jarosite (as confirmed by XRD; Fig. 2), resulting in the reaction being fitted to diffusion

through product film throughout the bioleaching period (Fig. 8a; Table 3). At higher  $\text{Ag}_2\text{S}$  concentration of 0.03 and 0.04%, on the other hand, surface chemical reaction was likely the rate-limiting step until the end (Fig. 8e, f; Table 3), suggesting that formation of trisilver arsenic sulfide layer (as well as ferric arsenate “outer” layer) around the enargite surface did not rate-limit the enargite dissolution. Rather, formation of trisilver arsenic sulfide was likely involved in the mechanism of facilitated enargite dissolution. At 0.005-0.02%  $\text{Ag}_2\text{S}$  concentrations, enargite dissolution was controlled by surface chemical reaction but only at the early stage (0-20 days at 0.005% and 0-40 days at 0.01-0.02%; Fig. 8b, c, d; Table 3) due to depletion of Ag.

#### 4. Conclusions

Based on the overall results obtained in this study, a proposed mechanism for Ag-catalyzed bioleaching of enargite concentrate was summarized in Fig. 9. The mechanism includes the formation of at least two types of secondary products (chalcocite and trisilver arsenic sulfide).

Chalcocite intermediate: Due to the low rest potential of  $\text{Ag}_2\text{S}$  (compared to those of enargite and pyrite), consumption of  $\text{Fe}^{3+}$  is more likely directed towards oxidation of  $\text{Ag}_2\text{S}$  to produce  $\text{Fe}^{2+}$  and  $\text{Ag}^+$ . Instead, oxidation of pyrite by  $\text{Fe}^{3+}$  is

355 suppressed (I). Addition of  $\text{Ag}_2\text{S}$  may also partially inhibit activity of Fe-oxidizing  
356 microorganisms (II). Due to (I) and (II),  $\text{Fe}^{2+}$  becomes more abundant than  $\text{Fe}^{3+}$  to  
357 maintain lower Eh to satisfy  $E_{\text{ox}}(\text{Cu}_2\text{S}) < E_h < E_c(\text{Ag}^+)$ . Consequently, enargite  
358 dissolution was enhanced via formation of  $\text{Cu}_2\text{S}$  intermediate, accompanied with  
359 production of  $\text{H}_2\text{S}$  which is rapidly removed by  $\text{Ag}^+$  to re-form  $\text{Ag}_2\text{S}$  (III). The resultant  
360  $\text{Cu}_2\text{S}$  is amenable to oxidation by  $\text{Fe}^{3+}$  to solubilize  $\text{Cu}^{2+}$  (IV).

361 Trisilver arsenic sulfide: Cu ion in the enargite structure is gradually substituted  
362 with  $\text{Ag}^+$  solubilized from  $\text{Ag}_2\text{S}$  to form an intermediate layer of  $(\text{Cu},\text{Ag})_3\text{AsS}_4$ .  
363 Eventually trisilver arsenic sulfide ( $\text{Ag}_3\text{AsS}_4$ ) covers the surface of enargite (V). The  
364 formation of this product film, however, does not impose a rate-limiting step.

365 The combination of the above reactions contributes to enhanced enargite  
366 bioleaching in the presence of  $\text{Ag}_2\text{S}$  as an effective Ag catalyst.

## Reference

Acevedo, F., Gentina, J.C. and García, N., 1998. CO<sub>2</sub> supply in the biooxidation of an enargite-pyrite gold concentrate. *Biotechnology Letters* 20, 257-259.

Ahonen, L. and Tuovinen, O.H., 1990. Catalytic effects of silver in the microbiological leaching of finely ground chalcopyrite-containing ore materials in shake flasks. *Hydrometallurgy* 24, 219-236.

Ballester, A., González, F., Blázquez, M.L. and Mier, J.L., 1990. The influence of various ions in the bioleaching of metal sulphides. *Hydrometallurgy* 23, 221-235.

Boekstein, A., Stadhouders, A.M., Stols, A.L.H. and Roomans, G.M., 1983. A comparison of ZAF-correction methods in quantitative X-ray microanalysis of light-element specimens. *Ultramicroscopy* 12, 65-68.

Córdova, R., Gómez, H., Real, S.G., Schrebler, R. and Vilche, J.R., 1997. Characterization of natural enargite/aqueous solution systems by electrochemical techniques. *Journal of the Electrochemical Society* 144, 2628-2636.

386

387 Escobar, B., Huenupi, E. and Wiertz, J.V., 1997. Chemical and biological leaching of  
388 enargite. *Biotechnology Letters* 19, 719-722.

389

390 Escobar, B., Huenupi, E., Godoy, I. and Wiertz, J.V., 2000. Arsenic precipitation in the  
391 bioleaching of enargite by *Sulfolobus* BC at 70°C. *Biotechnology Letters* 22, 205-209.

392

393 Fantauzzi, M., Elsener, B., Atzei, D., Lattanzi, P. and Rossi, A., 2007. The surface of  
394 enargite after exposure to acidic ferric solutions: an XPS/XAES study. *Surface and*  
395 *Interface Analysis* 39, 908-915.

396

397 Fantauzzi, M., Rossi, G., Elsener, B., Loi, G., Atzei, D. and Rossi, A., 2009. An XPS  
398 analytical approach for elucidating the microbially mediated enargite oxidative  
399 dissolution. *Analytical and bioanalytical chemistry* 393, 1931-1941.

400

401 Ghahremaninezhad, A., Asselin, E. and Dixon, D.G., 2010. Electrochemical evaluation  
402 of the surface of chalcopyrite during dissolution in sulfuric acid solution.  
403 *Electrochimica Acta* 55, 5041-5056.



404

405 Ghahremaninezhad, A., Dixon, D.G. and Asselin, E., 2013. Electrochemical and XPS  
406 analysis of chalcopyrite ( $\text{CuFeS}_2$ ) dissolution in sulfuric acid solution. *Electrochimica*  
407 *Acta* 87, 97-112.

408

409 Ghahremaninezhad, A., Radzinski, R., Gheorghiu, T., Dixon, D.G. and Asselin, E., 2015.  
410 A model for silver ion catalysis of chalcopyrite ( $\text{CuFeS}_2$ ) dissolution. *Hydrometallurgy*  
411 155, 95-104.

412

413 Goates, J.R., Cole, A.G., Gray, E.L. and Faux, N.D., 1951. Thermodynamic properties  
414 of silver sulfide. *Journal of the American Chemical Society* 73, 707-708.

415

416 Golyshina, O.V., Pivovarova, T.A., Karavaiko, G.I., Kondratéva, T.F., Moore, E.R.B.,  
417 Abraham, W.-R., Lünsdorf, H., Timmis, K.N., Yakimov, M.M. and Golyshin, P.N., 2000.  
418 *Ferroplasma acidiphilum* gen. nov., sp. nov., an acidophilic, autotrophic,  
419 ferrous-iron-oxidizing, cell-wall-lacking, mesophilic member of the *Ferroplasmaceae*  
420 fam. nov., comprising a distinct lineage of the Archaea. *International journal of*  
421 *systematic and evolutionary microbiology* 50, 997-1006.

422

423 Hackl, R.P., Dreisinger, D.B., Peters, E. and King, J.A., 1995. Passivation of  
424 chalcopyrite during oxidative leaching in sulfate media. Hydrometallurgy 39, 25-48.

425

426 Hiroyoshi, N., Arai, M., Miki, H., Tsunekawa, M. and Hirajima, T., 2002. A new  
427 reaction model for the catalytic effect of silver ions on chalcopyrite leaching in sulfuric  
428 acid solutions. Hydrometallurgy 63, 257-267.

429

430 Hseu, T.M. and Rechnitz, G.A., 1968. Analytical study of a sulfide ion-selective  
431 membrane electrode in alkaline solution. Analytical chemistry 40, 1054-1060.

432

433 Lee, J., Acar, S., Doerr, D.L. and Brierley, J.A., 2011. Comparative bioleaching and  
434 mineralogy of composited sulfide ores containing enargite, covellite and chalcocite by  
435 mesophilic and thermophilic microorganisms. Hydrometallurgy 105, 213-221.

436

437 Majima, H., 1969. How oxidation affects selective flotation of complex sulphide ores.  
438 Canadian Metallurgical Quarterly 8, 269-273.

439

440 Marambio-Jones, C. and Hoek, E.M., 2010. A review of the antibacterial effects of  
441 silver nanomaterials and potential implications for human health and the environment.  
442 Journal of Nanoparticle Research 12, 1531-1551.

443

444 Miki, H., Iguchi, A., Hirajima, T. and Sasaki, K., 2016. Catalytic effect of silver on  
445 arsenic-containing copper sulfide dissolution in acidic solution. Hydrometallurgy 162,  
446 1-8.

447

448 Muñoz, J.A., Blázquez, M.L., González, F., Ballester, A., Acevedo, F., Gentina, J.C. and  
449 González, P., 2006. Electrochemical study of enargite bioleaching by mesophilic and  
450 thermophilic microorganisms. Hydrometallurgy 84, 175-186.

451

452 Muñoz, J.A., Dreisinger, D.B., Cooper, W.C. and Young, S.K., 2007. Silver-catalyzed  
453 bioleaching of low-grade copper ores. Part I: Shake flasks tests. Hydrometallurgy 88,  
454 3-18.

455

456 Nazari, G., Dixon, D.G. and Dreisinger, D.B., 2012. The role of silver-enhanced pyrite  
457 in enhancing the electrical conductivity of sulfur product layer during chalcopyrite

458 leaching in the Galvanox<sup>TM</sup> process. Hydrometallurgy 113-114, 177-184.

459

460 Padilla, R., Fan, Y. and Wilkomirsky, I., 2001. Decomposition of enargite in nitrogen

461 atmosphere. Canadian Metallurgical Quarterly 40, 335-342.

462

463 Padilla, R., Jerez, O. and Ruiz, M.C., 2015. Kinetics of the pressure leaching of enargite

464 in FeSO<sub>4</sub>–H<sub>2</sub>SO<sub>4</sub>–O<sub>2</sub> media. Hydrometallurgy 158, 49-55.

465

466 Rivera-Vasquez, B.F. and Dixon, D., 2015. Rapid atmospheric leaching of enargite in

467 acidic ferric sulfate media. Hydrometallurgy 152, 149-158.

468

469 Ruiz, M.C., Vera, M.V. and Padilla, R., 2011. Mechanism of enargite pressure leaching

470 in the presence of pyrite. Hydrometallurgy 105, 290-295.

471

472 Safarzadeh, M.S. and Miller, J.D., 2014. Reaction of enargite (Cu<sub>3</sub>AsS<sub>4</sub>) in hot

473 concentrated sulfuric acid under an inert atmosphere. Part I: Enargite concentrate.

474 International Journal of Mineral Processing 128, 68-78.

475

476 Sasaki, K., Nakamuta, Y., Hirajima, T. and Tuovinen, O.H., 2009. Raman  
477 characterization of secondary minerals formed during chalcopyrite leaching with  
478 *Acidithiobacillus ferrooxidans*. Hydrometallurgy 95, 153-158.

479

480 Sasaki, K., Takatsugi, K., Kaneko, K., Kozai, N., Ohnuki, T., Tuovinen, O.H. and  
481 Hirajima, T., 2010. Characterization of secondary arsenic-bearing precipitates formed in  
482 the bioleaching of enargite by *Acidithiobacillus ferrooxidans*. Hydrometallurgy 104,  
483 424-431.

484

485 Sasaki, K., Takatsugi, K. and Hirajima, T., 2011. Effects of initial  $\text{Fe}^{2+}$  concentration  
486 and pulp density on the bioleaching of Cu from enargite by *Acidianus brierleyi*.  
487 Hydrometallurgy 109, 153-160.

488

489 Takatsugi, K., Sasaki, K. and Hirajima, T., 2011. Mechanism of the enhancement of  
490 bioleaching of copper from enargite by thermophilic iron-oxidizing archaea with the  
491 concomitant precipitation of arsenic. Hydrometallurgy 109, 90-96.

492

493 Tanaka, M., Yamaji, Y., Fukano, Y., Shimada, K., Ishibashi, J.-I., Hirajima, T., Sasaki,

494 K., Sawada, M. and Okibe, N., 2015. Biooxidation of gold-, silver, and  
495 antimony-bearing highly refractory polymetallic sulfide concentrates, and its  
496 comparison with abiotic pretreatment techniques. Geomicrobiology Journal 32,  
497 538-548.

498

499 Wadsworth, M.E. and Sohn, H.Y., 1979. Rate processes of extractive metallurgy.  
500 Plenum Press.

501

502 Warren, G.W., Wadsworth, M.E. and El-Raghy, S.M., 1982. Passive and transpassive  
503 anodic behavior of chalcopyrite in acid solutions. Metallurgical Transactions B 13,  
504 571-579.

505

506 Watkin, E.L.J., Keeling, S.E., Perrot, F.A., Shiers, D.W., Palmer, M.-L. and Watling,  
507 H.R., 2009. Metals tolerance in moderately thermophilic isolates from a spent copper  
508 sulfide heap, closely related to *Acidithiobacillus caldus*, *Acidimicrobium ferrooxidans*  
509 and *Sulfobacillus thermosulfidooxidans*. Journal of industrial microbiology &  
510 biotechnology 36, 461-465.

511

512 Watling, H.R., Perrot, F.A. and Shiers, D.W., 2008. Comparison of selected  
513 characteristics of *Sulfobacillus* species and review of their occurrence in acidic and  
514 bioleaching environments. Hydrometallurgy 93, 57-65.  
515

## Legends

### Fig. 1

Changes in the total soluble Cu concentration (a), total soluble As concentration (b), total soluble Fe concentration (c), Fe(II) concentration (d), solution redox potential (e) and cell density (f) during bioleaching of enargite concentrate at 0% (●), 0.005% (■), 0.01% (▲), 0.02% (▼), 0.03% (○) or 0.04% (□) of Ag<sub>2</sub>S. Cell densities are shown as mixed population of *At. caldus* KU, *Am. ferrooxidans* ICP, *Sb. sibiricus* N1 and *Fp. acidiphilum* Y. Data points are mean values from duplicate cultures. Error bars depicting averages are not visible in some cases as they are smaller than the data point symbols.

### Fig. 2

X-ray diffraction patterns of original enargite concentrate (a) and bioleached residues (b-g) recovered on day 72 from cultures containing 0% (b), 0.005% (c), 0.01% (d), 0.02% (e), 0.03% (f) or 0.04% (g) of Ag<sub>2</sub>S. ▲: enargite (Cu<sub>3</sub>AsS<sub>4</sub>; PDF No. 00-035-0775), ○: pyrite (FeS<sub>2</sub>; PDF No. 00-042-1340), ■: quartz (SiO<sub>2</sub>; PDF No. 01-070-3755), ◇: jarosite (K(Fe<sub>3</sub>(SO<sub>4</sub>)<sub>2</sub>(OH)<sub>6</sub>); PDF No. 01-076-0629).

### Fig. 3



X-ray diffraction patterns of red precipitates selectively collected from the bioleaching culture containing 0.04% Ag<sub>2</sub>S. T: trisilver arsenic sulfide (Ag<sub>3</sub>AsS<sub>4</sub>; PDF No. 01-089-1370), En: enargite (Cu<sub>3</sub>AsS<sub>4</sub>; PDF No. 00-035-0775), Py: pyrite (FeS<sub>2</sub>; PDF No. 00-042-1340), Q: quartz (SiO<sub>2</sub>; PDF No. 01-070-3755).

**Fig. 4**

Microbial population structure on day 15, 30 and 72 in bioleaching cultures of enargite concentrate at 0% and 0.04% of Ag<sub>2</sub>S. N1, ICP and KU indicate *Am. ferrooxidans* ICP, *Sb. sibiricus* N1 and *At. caldus* KU, respectively.

**Fig. 5**

Relationship between the Cu leaching rate and Eh value in bioleaching of enargite concentrate at 0.005% (■), 0.01% (▲), 0.02% (▼), 0.03% (○) and 0.04% (□) of Ag<sub>2</sub>S. Sterile controls at 0.02% Ag<sub>2</sub>S (◆) are also included. Data sets obtained from day 15 to 35 were employed.

**Fig. 6**

EPMA elemental mapping of enargite concentrate residue bioleached for 72 days with

0.04% Ag<sub>2</sub>S: The backscattered electron image at 2000-fold magnification (a) was mapped for Ag (b), Cu (c), As (d), S (e) and Fe (f). The surface of an enargite grain is covered with Ag-containing secondary mineral (solid arrow), on which deposition of ferric arsenate is observed (broken arrow).

**Fig. 7**

Backscattered electron image of an enargite grain bioleached for 72 days with 0.04% Ag<sub>2</sub>S at the 2000-fold magnification. Cross point 1-4 indicate the beam spot positions for quantitative analysis (results summarized in Table 2).

**Fig. 8**

Kinetic modeling on bioleaching of enargite concentrate at different Ag<sub>2</sub>S concentrations: (a) 0%, (b) 0.005%, (c) 0.01%, (d) 0.02%, (e) 0.03% and (f) 0.04%. Solid and open symbols indicate the fitting data to surface chemical reaction  $(1 - X)^{1/3} = k_r t$  and diffusion through product film  $(1 - 3(1 - X)^{2/3} + 2(1 - X) = k_d t)$ , respectively. Linear lines were drawn where R<sup>2</sup> values were calculated to be > 0.99.

**Fig. 9**

Schematic image illustrating the proposed mechanism of Ag-catalyzed bioleaching of enargite concentrate.

**Supplemental Fig. 1**

Relationship between solution redox potential (Eh) and thermodynamically calculated equilibrium concentration of  $\text{Ag}^+$ .

**Table 1**

PCR and Real-Time PCR primers used in this study

**Table 2**

EPMA quantitative analysis of secondary minerals formed on the enargite surface after bioleaching

Footnote:

\* No. 1-4 indicate the cross points 1-4 in Fig. 7, respectively.

**Table 3**

$R^2$  and  $k$  values calculated using the kinetic model of surface chemical reaction and diffusion through product film

Footnote: Shadowed cells ( $R^2 > 0.99$ ) indicate which one of the two models fits the experimental data

### Supplemental Table 1

Values used for thermodynamic calculations to obtain  $E_c(\text{Cu}^{2+})$ ,  $E_c(\text{Ag}^+)$  and  $E_{\text{ox}}(\text{Cu}_2\text{S})$ , assuming that the total soluble As concentration equals to the As(III) concentration

Footnotes:

<sup>a</sup>  $E_c(\text{Cu}^{2+})$ ,  $E_c(\text{Ag}^+)$  and  $E_{\text{ox}}(\text{Cu}_2\text{S})$  were calculated by using Eq. i, ii and iii, respectively.

$$E_c(\text{Cu}^{2+}) = E_c^0(\text{Cu}^{2+}) + \frac{RT}{14F} \ln \frac{(\alpha_{\text{Cu}^{2+}})^{10}}{(\alpha_{\text{H}_3\text{AsO}_3})^2 (\alpha_{\text{H}^+})^6} \quad (\text{Eq. i})$$

$$E_c(\text{Ag}^+) = E_c^0(\text{Ag}^+) + \frac{RT}{4F} \ln \frac{(\alpha_{\text{Ag}^+})^{10}}{(\alpha_{\text{H}_3\text{AsO}_3})^2 (\alpha_{\text{H}^+})^6} \quad (\text{Eq. ii})$$

$$E_{\text{ox}}(\text{Cu}_2\text{S}) = E_{\text{ox}}^0(\text{Cu}_2\text{S}) + \frac{RT}{4F} \ln (\alpha_{\text{Cu}^{2+}})^2 \quad (\text{Eq. iii})$$

$R$ : gas constant (J/Kmol)

$T$ : temperature (K)

$F$ : Faraday constant (C/mol)

$\alpha_i$ : activity of species  $i$

Here,  $E_c^0(\text{Cu}^{2+})$ ,  $E_c^0(\text{Ag}^+)$  and  $E_{\text{ox}}^0(\text{Cu}_2\text{S})$  indicate the standard redox potentials (V) of

Eq. 7, 10 and 8 calculated by Eq. iv, v and vi, respectively.

$$E_c^0(\text{Cu}^{2+}) = -\frac{1}{14F}(8\Delta G_{\text{Cu}_2\text{S}}^0 + 2\Delta G_{\text{H}_3\text{AsO}_3}^0 + 6\Delta G_{\text{H}^+}^0 - 2\Delta G_{\text{Cu}_3\text{AsS}_4}^0 - 6\Delta G_{\text{H}_2\text{O}}^0 - 10\Delta G_{\text{Cu}^{2+}}^0) \quad (\text{Eq. iv})$$

$$E_c^0(\text{Ag}^+) = -\frac{1}{4F}(3\Delta G_{\text{Cu}_2\text{S}}^0 + 5\Delta G_{\text{Ag}_2\text{S}}^0 + 2\Delta G_{\text{H}_3\text{AsO}_3}^0 + 6\Delta G_{\text{H}^+}^0 - 2\Delta G_{\text{Cu}_3\text{AsS}_4}^0 - 6\Delta G_{\text{H}_2\text{O}}^0 - 10\Delta G_{\text{Ag}^+}^0) \quad (\text{Eq. v})$$

$$E_{\text{ox}}^0(\text{Cu}_2\text{S}) = -\frac{1}{4F}(\Delta G_{\text{Cu}_2\text{S}}^0 - 2\Delta G_{\text{Cu}^{2+}}^0 - \Delta G_{\text{S}^{0}}^0) \quad (\text{Eq. vi})$$

$\Delta G_i^0$  indicates the standard Gibbs free energy of species  $i$  and those used for calculation are listed in Supplemental Table 3. The values of  $E_c^0(\text{Cu}^{2+})$ ,  $E_c^0(\text{Ag}^+)$  and  $E_{\text{ox}}^0(\text{Cu}_2\text{S})$  were thus calculated to be 0.628, 1.867 and 0.562 V, respectively.

<sup>b</sup> Since Ag concentrations in leachates were below the detection limit of ICP-OES, they were thermodynamically calculated as follows and listed in Supplemental Tables 1 and 2. Dissolution of  $\text{Ag}_2\text{S}$  in bioleaching culture (Eq. vii) and the equilibrium potential of Eq. vii (Eq. viii) are expressed as below (Miki et al., 2016).



$$E_{\text{ox}}(\text{Ag}_2\text{S}) = E_{\text{ox}}^0(\text{Ag}_2\text{S}) + \frac{RT}{F} \ln(\alpha_{\text{Ag}^+}) \quad (\text{Eq. viii})$$

$E_{\text{ox}}(\text{Ag}_2\text{S})$  (“oxidation potential”): the equilibrium redox potential for oxidation of  $\text{Ag}_2\text{S}$  to  $\text{Ag}^+$  (Eq. vii)

$E_{\text{ox}}^0(\text{Ag}_2\text{S})$ : the standard redox potential of Eq. vii, as calculated by Eq. ix.

$$E_{\text{ox}}^0(\text{Ag}_2\text{S}) = -\frac{1}{2F}(\Delta G_{\text{Ag}_2\text{S}}^0 - 2\Delta G_{\text{Ag}^+}^0 - \Delta G_{\text{S}^0}^0) \quad (\text{Eq. ix})$$

Based on Eq. viii, when the activity coefficient is defined as 1, the Ag concentration was calculated by the function of  $E_{\text{ox}}(\text{Ag}_2\text{S})$  as shown in Supplemental Fig. 1.

### Supplemental Table 2

Values used for thermodynamic calculations to obtain  $E_{\text{c}}(\text{Cu}^{2+})$ ,  $E_{\text{c}}(\text{Ag}^+)$  and  $E_{\text{ox}}(\text{Cu}_2\text{S})$ , assuming that the As(III) concentrations is negligible ( $10^{-5}$  M). The calculation methods are described in Supplemental Table 1.

### Supplemental Table 3

Standard Gibbs free energy of each species used for thermodynamic calculation described in Supplemental Table 1

Foot notes:

<sup>a</sup> Padilla et al. (2001)

<sup>b</sup> Outokumpu (HSC Chemistry 5 software)

643    **Acknowledgements**

644            Enargite concentrate was kindly provided by JX Nippon Mining & Metals. K.  
645    O. is grateful for financial support provided by the Kyushu University Advanced  
646    Graduate Program in Global Strategy for Green Asia.